Effect of humidity on the absorption continua of CO 2 and N 2 near 4 μ m: Calculations, comparisons with measurements, and consequences for atmospheric spectra

Jean-Michel Hartmann, Christian Boulet, Duc Dung Tran, Ha Tran, Yury Baranov

Effect of humidity on the absorption continua of CO_2 and N_2 near 4 μm: Calculations, comparisons with measurements, and consequences for atmospheric spectra

Jean-Michel Hartmann, Christian Boulet, Duc Dung Tran, Ha Tran, and Yury Baranov

Citation: The Journal of Chemical Physics **148**, 054304 (2018); doi: 10.1063/1.5019994
View online: https://doi.org/10.1063/1.5019994
View Table of Contents: http://aip.scitation.org/toc/jcp/148/5
Published by the American Institute of Physics

Effect of humidity on the absorption continua of CO_2 and N_2 near 4 μm: Calculations, comparisons with measurements, and consequences for atmospheric spectra

Jean-Michel Hartmann,[1,a)] Christian Boulet,[2] Duc Dung Tran,[3] Ha Tran,[3] and Yury Baranov[4]
[1]*Laboratoire de Météorologie Dynamique/IPSL, CNRS, Ecole Polytechnique, Université Paris-Saclay, 91128 Palaiseau, France*
[2]*Institut des Sciences Moléculaires d'Orsay, CNRS, Université Paris-Sud, Université Paris-Saclay, Orsay F-91405, France*
[3]*Laboratoire de Météorologie Dynamique, IPSL, UPMC Univ. Paris 06, Ecole Polytechnique, Ecole Normale Supérieure, Sorbonne Universités, Université Paris-Saclay, PSL Research University, CNRS, 4 Place Jussieu, 75005 Paris, France*
[4]*SPA "Typhoon," Institute of Experimental Meteorology, 4 Pobeda St., Obninsk, Kaluga Region 249034, Russia*

(Received 19 December 2017; accepted 18 January 2018; published online 6 February 2018)

We present a theoretical study of the effects of collisions with water vapor molecules on the absorption, around 4 μm, in both the high frequency wing of the CO_2 ν_3 band and the collision-induced fundamental band of N_2. Calculations are made for the very first time, showing that predictions based on classical molecular dynamics simulations enable, without adjustment of any parameter, very satisfactory agreement with the few available experimental determinations. This opens the route for a future study in which accurate temperature-dependent (semi-empirical) models will be built and checked through comparisons between computed and measured atmospheric spectra. This is of interest since, as demonstrated by simulations, neglecting the humidity of air can lead to significant modifications of the atmospheric transmission (and thus also emission) between 2000 and 2800 cm^{-1}. *Published by AIP Publishing.* https://doi.org/10.1063/1.5019994

I. INTRODUCTION

To the best of our knowledge, radiative transfer codes for studies of the Earth's atmosphere have, so far, disregarded most (if not all) of the effects of the presence of water vapor on the absorption spectra of other gases. There are several reasons for this situation: (i) The first is that the temperature-dependent pressure-broadening coefficients of the lines of the absorbing gas resulting from collisions with H_2O are not provided in the currently used databases.[1,2] Although some data are available (e.g., Refs. 3–5 and those therein), these databases still provide complete sets of values for mixtures with dry air only. An effort is underway to extend the High-Resolution Transmission Molecular Absorption (HITRAN) database and some broadening coefficients by H_2, He, and CO_2, but not H_2O so far, are now available.[1,6] (ii) The second is due to the relatively small mole fraction of H_2O in the Earth's atmosphere and the fact that the broadening coefficients by H_2O and dry air are not so different,[3–5] the errors induced by using only dry-air broadenings remain of the order of one percent or less. This assumption can thus be used in most atmospheric studies, where the errors that it induces are masked by other sources of uncertainty, except for those which aim at an extremely high accuracy. This is the case, for instance, of the space-borne remote sensing of greenhouse gases[7–9] for which the broadening effect of collisions with H_2O may have to be taken into account for very humid atmospheres. (iii) Finally, when one considers the broadband continua resulting from collision-induced absorption (CIA) (e.g., those of N_2 in the far infrared and near 4 μm) or from the far line wings (e.g., those of the intense ν_2 and ν_3 bands of CO_2), no model is available (except for H_2O itself[10]). The influence of humidity is, thus again, supposed to be negligible and all computations of the atmospheric continua of gases other than H_2O, and associated retrieval exercises, are made for dry air.

This last assumption may induce significant errors in the region around 4 μm, which is used for various observations (e.g., Refs. 11–16), where the Earth's atmospheric absorption is largely due to N_2 continuum with a weaker contribution of the CO_2 far line wings. Indeed, Ref. 17 shows that, with respect to N_2–N_2 (or N_2-air) collisions, N_2–H_2O interactions considerably enhance the collision-induced absorption in the fundamental band of N_2 (a factor of nearly ten on the integrated band area). A similar result is obtained[18,19] for the high frequency wing of the CO_2 ν_3 band, where the binary absorption coefficient for CO_2–H_2O is, around 2500 cm^{-1}, about one order of magnitude larger than that for CO_2–N_2. As can thus be expected (and is demonstrated in this paper), significant errors in computations of atmospheric spectra are induced by neglecting the effect of collisions with water vapor on the continua between roughly 3.6 and 4.2 μm. Unfortunately, there is no model so far and the (very few) measured data remain insufficient for atmospheric spectra calculations. Indeed, they were all obtained above 50 °C and provide no reliable information on the temperature dependence. This results

a)Author to whom correspondence should be addressed: jean-michel.hartmann@lmd.polytechnique.fr

from the optical thicknesses attainable in laboratory experiments, which are limited, for the considered spectral region, by both the path lengths of the cells and the H_2O saturation pressure. Indeed, while very long optical paths can be obtained using high finesse cavities and cavity enhanced absorption spectroscopy (CEAS) or cavity ringdown spectroscopy (CRDS) techniques, the wavelengths that can be studied remain practically limited to below ≈2 μm due to mirror technology limits. These two constraints make laboratory experiments below ≈300 K extremely difficult if not infeasible. Using theoretical calculations to complete the available experimental information is thus, today, the only solution.

The present paper tests the ability of some theoretical models to predict the CO_2–H_2O and N_2–H_2O continua near 4 μm by comparing computed results with the available measurements. This is a first step before producing data at temperatures relevant for the Earth's atmosphere and testing them by comparisons between measured and computed atmospheric spectra, which will be the subject of a future work. For the predictions, rigorous quantum mechanical approaches cannot be used for the considered molecular systems since they are far too complex. Hence, we here mostly use Classical Molecular Dynamics Simulations (CMDSs) with which very satisfactory agreements with measured values are obtained for both CO_2 and N_2 in H_2O vapor, opening the route to more extensive temperature-dependent predictions. The remainder of this paper is divided into four parts. Section II is devoted to the high frequency wing of the H_2O-broadened CO_2 ν_3 band. It describes the theoretical approach and its input data and presents comparisons between calculated and experimental results. Similarly, the methods used for computations of the H_2O-induced absorption by N_2 in the fundamental band and comparisons between predictions and measurements are presented in Sec. III. The consequences of humidity on the atmospheric absorptions by CO_2 and N_2 around 4 μm are then simulated and discussed in Sec. IV before some concluding remarks and directions for future studies (Sec. V).

II. THE H_2O-BROADENED HIGH FREQUENCY WING OF THE CO_2 ν_3 BAND

A. Classical molecular dynamics simulations and input data

The binary absorption coefficient of CO_2 colliding with water vapor in the region of the ν_3 band was calculated using a combination of the methods described in Refs. 20–22, as explained below.

1. Molecular orientations and positions

In Refs. 18 and 19, the purely binary CO_2–H_2O density-normalized absorption coefficient in the region beyond the ν_3 band (2400-2600 cm^{-1}) was experimentally determined. For this, the contributions of local CO_2 and H_2O lines as well as those of the CO_2-broadened ν_3 wing and of the water-vapor continuum were subtracted from measured spectra. The resulting sets of values deduced from measurements for various mixtures were then divided by the product of the corresponding H_2O and CO_2 densities and averaged. This exercise provides a binary absorption, normalized to H_2O and CO_2 partial densities of 1 amagat (Am, with 1 Am = 2.69×10^{19} molecule/cm^3), that results only from interactions between CO_2 and H_2O molecules, all effects of local lines and of CO_2–CO_2 and H_2O–H_2O collisions having been removed. In order to compute this quantity, Classical Molecular Dynamics Simulations (CMDSs) of the rotational and translational motions of an ensemble of CO_2 and H_2O gas molecules, treated as rigid rotors, were carried as described in Refs. 20 and 21. This was made for nearly fifty millions of molecules of a 50% CO_2 + 50% H_2O mixture with partial densities of 1 Am for each species and the temperature (323 K) of the experiments.[18] Under such conditions, the collisions are binary and only the CO_2–H_2O interactions were taken into account, consistently with what was deduced from measurements, disregarding the CO_2–CO_2 and H_2O–H_2O ones by setting the associated intermolecular potentials to zero. Within these assumptions, the rotational and translational evolutions of all molecules were computed for 30 ps, after a thermalization time of 10 ps, with a time step of 1 fs. The forces and torques applied to each molecule in CO_2–H_2O colliding pairs were computed from a site-site intermolecular potential constructed as follows: Coulombic forces were calculated from electric charges distributed in the H_2O and CO_2 molecules as described in Refs. 24 and 25, respectively. Site-site repulsive and dispersive forces were then added, following Ref. 26.

2. Dipole moments

The CMDSs described above provide the positions and orientations of all molecules at all times. From this knowledge, the absorption coefficient in the region of the CO_2 ν_3 band was computed following Ref. 22. Namely, the time evolution of the intrinsic (i.e., that tied to the molecule, that results from its asymmetric vibration and not from its interaction with a collision partner) dipole vector of each CO_2 molecule (which lies on the molecular axis for the parallel ν_3 band) was computed from knowledge of the molecular axis orientation.[22] At the same time, the interaction-induced dipole in each CO_2–H_2O pair was calculated as done in Refs. 22 and 27, but here limited to the contribution of the static isotropic polarizability of H_2O, $\langle v = 0 | \alpha_{H_2O} | v = 0 \rangle$ = 9.9 a.u. (value used in Ref. 28 which is representative of the experimental and theoretical results reported in Refs. 29–31 and "a.u." meaning "atomic units"), in the field of the $^{12}CO_2$ vibrating dipole, $\langle v = \nu_3 | \mu_{CO_2} | v = 0 \rangle = -0.13$ a.u. (value used in Ref. 22 which is consistent with predictions and measurements reported in Refs. 32–34). Several other terms[35] involving the anisotropy of the polarizability (γ_{H_2O}) of H_2O have been neglected because γ_{H_2O} is very small,[29–31] while those associated with vibrational matrix elements $\langle v = \nu_3 | X_{CO_2} | v = 0 \rangle$ (for $X = \alpha$, γ and the quadrupole Θ) are disregarded because they vanish due to symmetry considerations. The time autocorrelation function (ACF) of the full dipole was then computed including, as in Ref. 22, three contributions: The purely intrinsic one, the purely induced one, and the cross terms (intrinsic-induced and induced-intrinsic) coming from the so-called intra-collisional interference.

3. Absorption spectrum

Finally, the spectrum was computed[22,36] from the Fourier transform of the full dipole ACF, multiplied by the proper radiative factor, shifted by the CO_2 ν_3 vibrational frequency (2349 cm^{-1}) and scaled by the detailed balance correction $\exp(2\pi c\Delta\sigma/2k_BT)$, where $\Delta\sigma$ is the distance from the band center. Following Ref. 22, the minor but not fully negligible contributions from the ν_3 band of $^{13}CO_2$ and the $\nu_3 + \nu_2 - \nu_2$ band of $^{12}CO_2$ were included in the same way.

B. Comparison with measured values

Measured binary absorption coefficients (normalized by the product of the CO_2 and collision partner densities) beyond the band head of the $^{12}CO_2$ ν_3 band for pure CO_2 and CO_2 in H_2O are compared in Fig. 1 with the associated CMDS results from Ref. 22 (in which CO_2–CO_2 interactions were of course taken into account) and the present work, respectively. As can be seen, the computations do quite well predict the magnitude and shape of both continua, despite that no parameter was adjusted. In particular, the fact that CO_2–H_2O collisions significantly enhance the absorption with respect to CO_2–CO_2 interactions, with a ratio that increases with the detuning from the band center (at 2349 cm^{-1}), is reproduced. Note that although a large number of molecules were treated in the CMDS, the calculated results (Fig. 1) still carry a significant "noise." This results from the fact that the predictions in this region, of very weak absorption with respect to that near the ν_3 band center, are extremely sensitive to the exhaustivity with which the phase space is spanned and sampled.[23] It is worth mentioning that the calculation of the H_2O-broadened

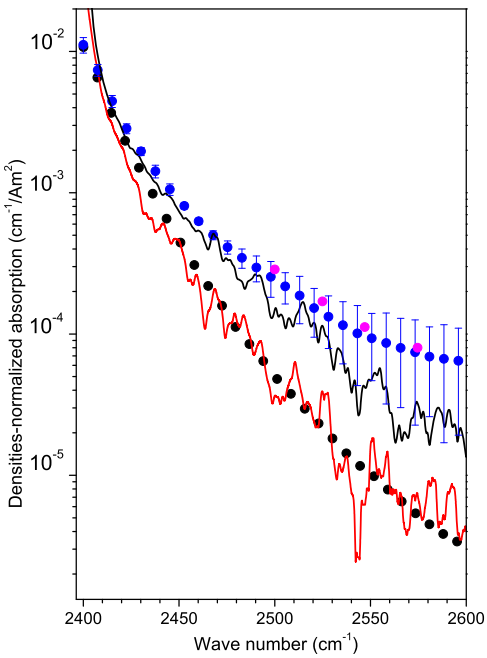

FIG. 1. Measured (symbols) and computed (lines) binary absorption coefficients beyond the ν_3 band head for pure CO_2 at 296 K (black circles are experiments from Ref. 37 and the red line denotes computed values from Ref. 22) and for CO_2 in H_2O at 323 K (blue and magenta circles are experiments from Refs. 18 and 19, while the present CMDS-computed results are the black line).With respect to the values given in Ref. 18, the error bars have been multiplied by 1.96 in order to represent the 95% confidence interval.

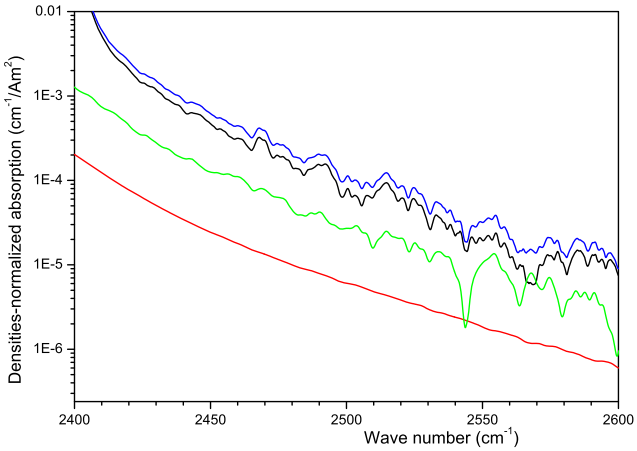

FIG. 2. Calculated dipole contributions to the CO_2–H_2O binary absorption coefficient beyond the ν_3 band head at 323 K. The lines denote (see text) results obtained for PP (black), II (red), PI + IP (green), and for the total PP + II + PI + IP (blue).

CO_2 far wing in Fig. 1 is the first one ever made. Considering the extreme complexity of the problem, the results obtained are, in our opinion, very satisfactory, although the difference between the predictions and measurements for CO_2 in H_2O increases with frequency and the distance from band center. Concerning this increase, we have no clear explanation, but it may come from the intermolecular potential since the calculated values in the far band wings are very sensitive to details of the description of collisions at short time (and thus distance) scales.

Since the full dipole involves both an intrinsic, coming from the asymmetric vibration, and an interaction-induced component, its ACF results from the addition of a purely intrinsic ($\langle\vec{\mu}^{P}(t).\vec{\mu}^{P}(0)\rangle$), a purely induced ($\langle\vec{\mu}^{I}(t).\vec{\mu}^{I}(0)\rangle$), and a cross ($\langle\vec{\mu}^{P}(t).\vec{\mu}^{I}(0) + \vec{\mu}^{I}(t).\vec{\mu}^{P}(0)\rangle$) term. Figure 2 presents their respective contributions, denoted as PP, II, and PI + IP. This shows that, for CO_2–H_2O, the purely induced term is practically negligible (~4% of the total) while the cross term (intra-collisional interference) is not (~20% of the total), a situation close to that for pure CO_2.[22]

III. THE N_2 FUNDAMENTAL BAND INDUCED BY COLLISIONS WITH H_2O

A. Classical molecular dynamics simulations and input data

The binary absorption coefficient of N_2 colliding with H_2O in the region of the fundamental band was calculated using a combination of the methods described in Refs. 20, 21, 27, and 38, as explained below.

1. Molecular orientations and positions

The molecular orientations and positions were obtained as described in Sec. II A 1 by replacing CO_2 by N_2 and setting the temperature to 352 K, which is one of the experiments.[17] The method used and the N_2–H_2O intermolecular potential (including Coulombic, repulsive, and dispersive forces) retained are described in Ref. 21. As done for CO_2 (cf. Sec. II A 1), N_2 and H_2O densities of 1 Am were used and the N_2–N_2

and H_2O–H_2O potentials were set to zero since Ref. 17 provides experimental values of the purely binary and density normalized contribution to the absorption.

2. Dipole moments

The dipole moment induced in colliding N_2–H_2O pairs, that leads to absorption in the fundamental band of N_2, was computed from knowledge of the positions and orientations of the molecules following the method described in Refs. 27 and 38. For this, we limited the induction terms to those associated with the following: (i) The isotropic and anisotropic polarizabilities of N_2 ($\langle v=0|\,\alpha_{N_2}|v=1\rangle$ = 0.375 a.u. and $\langle v=0|\,\gamma_{N_2}|v=1\rangle$ = 0.428 a.u.[38]) in the field of the static dipole of H_2O ($\langle v=0|\,\mu_{H_2O}|v=0\rangle$ = 0.73 a.u.; see Ref. 30 and those therein) which is carried by the vector in between the two O–H bonds. (ii) The static isotropic polarizability of H_2O, $\langle v=0|\alpha_{H_2O}|v=0\rangle$ = 9.9 a.u. (see Sec. II A 2), in the electric fields of the N_2 quadrupole and hexadecapole, $\langle v=0|\,\Theta_{N_2}|v=1\rangle$ = 0.0583 a.u. and $\langle v=0|\,\Phi_{N_2}|v=1\rangle$ = –0.158 a.u.[38] Other terms,[35] such as those induced by the anisotropic polarizability of H_2O (γ_{H_2O}) in the fields of the N_2 quadrupole and hexadecapole, have been neglected because $\langle v=0|\,\gamma_{H_2O}|v=0\rangle$ is very small as mentioned in Sec. II A 2. In fact, tests show that the computed collision-induced absorption (CIA) is strongly dominated by the contributions associated with α_{N_2} and γ_{N_2} in the field of μ_{H_2O}. These represent 80% of the computed integrated area of the CIA band, thanks to the very large water vapor dipole and the broad range of intermolecular distances over which this induction mechanism is efficient.

3. Absorption spectrum

Finally, the spectrum was computed[27] from the Fourier transform of the full dipole ACF, multiplied by the proper radiative factor, shifted by the N_2 vibrational frequency, and scaled by the detailed balance correction $\exp(2\pi c\Delta\sigma/2k_BT)$, where $\Delta\sigma$ is the distance from the band center (2329 cm^{-1}).

B. Isotropic quantum model and K_2 line shape

CIA spectra have also been calculated for the N_2–H_2O pair in the region of the nitrogen fundamental by using the model of Ref. 39, which is much simpler and less expensive than the CMDS. We here give only the relevant information on the model, the reader being invited to consult Refs. 40–43 for more details. The approach used is based on the so-called isotropic approximation which neglects the effect of the intermolecular potential anisotropy and thus assumes that the molecules rotate freely at all times. This is the most severe weakness of the model but it has the considerable advantage to enable us to write the absorption in terms of a superposition of independent components. Indeed, the binary absorption coefficient (i.e., the absorption normalized by the product of the densities of the two molecular species, in cm^{-1}/Am^2) at wave number σ and temperature T is then given by

$$\alpha(\sigma) = \frac{4\pi^2}{3}\sigma\alpha_F n_0^2 a_0^5 \sum_k \sum_{i_1,f_1,i_2,f_2} S_k(T,i_1,f_1,i_2,f_2) \times G_k(T,\sigma-\sigma_{f_1 i_1}-\sigma_{f_2 i_2}), \quad (1)$$

where α_F is the fine structure constant, a_0 is the Bohr radius, and n_0 is the number density at standard temperature and pressure (i.e., at 1 Am). The index k identifies the various components of the induced dipole.[35] S_k is the corresponding strength for the $(i_1, i_2) \rightarrow (f_1, f_2)$ transition, where i and f denote the initial and final states and the indices 1 and 2 refer to N_2 and H_2O, respectively. Finally, $G_k(T,\sigma-\sigma_{f_1 i_1}-\sigma_{f_2 i_2})$ is a normalized profile discussed below.

As mentioned above, for the N_2–H_2O pair, the dominant induction mechanisms are the dipole-induced dipole components. Among these, an example is given by the dipole arising from the isotropic polarizability of N_2 (α_{N_2}) in the field of the H_2O dipole (μ_{H_2O}). The corresponding component is associated[35] with $k \equiv \lambda_1, \lambda_2, \Lambda$, $L = 0, 1, 1, 2$ and the line strength $S_k(T, i_1, f_1, i_2, f_1)$ is proportional to $\rho_{i_1}(T)\rho_{i_2}(T)\langle i_1|\alpha_{N_2}|f_1\rangle^2\langle i_2|\mu_{H_2O}|f_2\rangle^2$, where $\rho_i(T)$ is the relative population of level i. For N_2, the rovibrational matrix elements $\langle v=0, J|X|v=1, J'\rangle$ of the various tensors X retained (i.e., the isotropic and anisotropic polarizabilities and the electric quadrupole and hexadecapole; see Sec. III A 2), and the associated positions $\sigma_{f_1 i_1} = \sigma_{v=1,J'\leftarrow v=0,J}$ of the transitions, can be easily calculated for all needed values of the rotational quantum numbers J and J'. They have analytical expressions[43] in terms of the vibrational matrix elements $\langle v=0|X|v=1\rangle$, of the vibrational energy and of the rotational constants. For H_2O, with rotational quantum numbers J, K_a, and K_c, while the $\langle v=0, J, K_a, K_c|\alpha_{H_2O}|v=0, J', K'_a, K'_c\rangle = \alpha_{H_2O}\delta_{J,J'}\delta_{K_a,K'_a}\delta_{K_c,K'_c}$ is trivial, the terms $\langle v=0, J, K_a, K_c|\,\mu_{H_2O}\,|v=0, J', K'_a, K'_c\rangle$ cannot be easily computed. However, since they are directly involved in the integrated intensities of the absorption lines of the rotational band, they were deduced from the associated values provided by the HITRAN2012 database.[44] The latter also gives the positions $\sigma_{f_2 i_2} = \sigma_{v=0,J',K'_a,K'_c\leftarrow v=0,J,K_a,K_c}$ and the energies of the levels for the calculation of the relative populations $\rho_{v=0,JK_aK_c}(T)$. Note that, when the N_2–H_2O pair absorbs a photon and N_2 makes a vibrational transition, H_2O can be simultaneously deexcited rotationally. This corresponds, for this molecule, to a dipole transition at a negative frequency for which there is no data in HITRAN. However, since one has $\sigma_{f_2 i_2} = -\sigma_{i_2 f_2}$ and $\langle f_2|\,\mu_{H_2O}|i_2\rangle^2 = [(2J_{f_2}+1)/(2J_{i_2}+1)]\,\langle i_2|\,\mu_{H_2O}|f_2\rangle^2$, the needed parameters for the transition $f_2 \leftarrow i_2$ can be deduced from those for the $i_2 \leftarrow f_2$ line which is present in HITRAN.

Concerning the line shape, many models have been proposed, the most widely used being that of Birnbaum and Cohen.[45] We have preferred to retain here the so-called K_2 line shape[46] because it can be completely determined *a priori*. $G_n(T,\Delta\sigma)$, which is area normalized, is then given by

$$G_k(T,\Delta\sigma) = \frac{2}{3\pi\eta_k(T)}\left[\frac{\Delta\sigma}{\eta_k(T)}\right]^2\left[1+\exp\left(-\frac{hc\Delta\sigma}{k_BT}\right)\right]^{-1} \times K_2\left[\Delta\sigma/\eta_k(T)\right], \quad (2)$$

where K_2 denotes a modified Bessel function of the second kind and $\eta_k(T)$ is a temperature-dependent parameter. The latter can be determined[46] from the chosen isotropic intermolecular potential and dipole component k (i.e., λ_1, λ_2, Λ, and L). The associated values at 350 K, calculated for a 12-6

TABLE I. Computed values (in cm^{-1}) of the η_k parameters of the K_2 line shape at 350 K. See Sec. III A 2 for the definition and retained values of the tensors and Ref. 35 for the associated sets of λ_1, λ_2, Λ, L (indices 1 and 2 refer to N_2 and H_2O, respectively).

Tensors	$n \equiv \lambda_1, \lambda_2, \Lambda, L$	η_n
α_{N_2}, μ_{H_2O}	(0,1,1,2)	12.1
γ_{N_2}, μ_{H_2O}	(2,1,1,2), (2,1,2,2), (2,1,3,2)	12.1
Θ_{N_2}, α_{H_2O}	(2,0,2,3)	18.0
Φ_{N_2}, α_{H_2O}	(4,0,4,5)	26.4

Lennard-Jones potential (with ε = 97 K and σ = 3.28 A, consistent with the angular average of that used for the CMDS), are given in Table I for all retained components of the induced dipoles.

In summary, as for the CMDS of Sec. III A, this model contains no adjustable parameter and enables calculations of the CIA spectra for N_2–H_2O mixtures in the region of the N_2 fundamental band.

C. Comparisons with measured values

Measured collision-induced binary absorption coefficients (normalized by the product of the N_2 and collision partner densities) in the fundamental band of N_2 for pure N_2 and N_2 in H_2O are compared in the main panel of Fig. 3 with the associated CMDS results from Ref. 38 and the present work, respectively. As can be seen, the computations do well predict the magnitude and shape (except for the central region of the N_2–H_2O CIA which is discussed at the end of this section) of both continua, despite the fact that no parameter was adjusted. Just as experiments, calculations show that N_2–H_2O collisions significantly enhance the CIA with respect to N_2–N_2 interactions, with a ratio that strongly increases when going toward the wings. A good agreement is obtained for the integrated CIA areas, with measured values of 5.1×10^{-3} cm^{-2}/Am^2 for N_2–H_2O and 3.7×10^{-4} cm^{-2}/Am^2 for N_2–N_2 with associated CMDS predictions of 5.1×10^{-3} cm^{-2}/Am^2 and 3.2×10^{-4} cm^{-2}/Am^2, respectively. Finally, the inset of Fig. 3 demonstrates that CMDS predictions for N_2–H_2O at various temperatures are largely within the experimental uncertainties of such difficult experiments.

A comparison between experiments and theory for the N_2–H_2O CIA now including the predictions of the isotropic quantum model with the K_2 line shape is shown in the main panel of Fig. 4 (similar comparisons for pure N_2 can be found in Refs. 43 and 49). As can be seen, this approach significantly underestimates the absorption with an error of a factor of nearly two on the integrated CIA area. This is consistent with the results of previous similar calculations for N_2–H_2O,[42] but in opposition with the good agreement between experiments and predictions obtained[43,49] for pure N_2 and N_2 in O_2. These results can be explained by the use of the isotropic approximation in which one assumes that the colliding molecules interact through an isotropic intermolecular potential (which drives the translational motion while the molecules rotate freely). Indeed, for pure N_2 around room temperature, it was shown[50–52] that this approximation is very reasonable, thanks to the moderate anisotropy of N_2–N_2 interactions, explaining the quality of the predictions in Refs. 43 and 49. For N_2–H_2O collisions, a significantly different situation results from the very strong and anisotropic long-range quadrupole-dipole interaction. In this case, the isotropic approximation leads to a significant underestimation of the CIA (as also predicted for pure CO_2[50,53] where quadrupole-quadrupole interactions are strong). This is demonstrated by the inset in Fig. 4 which shows that the CMDS results calculated assuming isotropic interactions are about twice smaller than those (shown in Fig. 3 and reproduced in the main panel of Fig. 4) obtained when the anisotropy is taken into account. Furthermore, the integrated CIA area of these isotropic CMDS predictions (3.32×10^{-3} cm^{-2}/Am^2) is also perfectly consistent with that (3.23×10^{-3} cm^{-2}/Am^2)

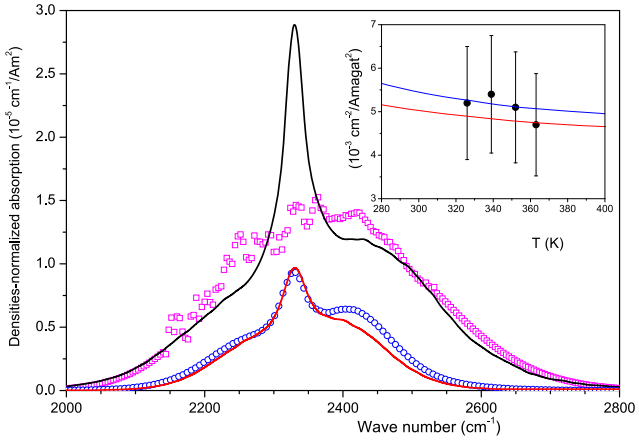

FIG. 3. Main panel: Measured (symbols) and CMDS-computed (lines) binary collision-induced absorption coefficients in the fundamental band of N_2. The experimental[47,48] and CMDS-calculated[38] spectra for pure N_2 at 362 K, both multiplied by 5, are represented by the blue circles and the red line, respectively. The measured[17] and CMDS-calculated spectra for N_2 in H_2O at 352 K are the magenta squares and the black line, respectively. Inset: Integrated N_2–H_2O CIA area versus temperature. The symbols and red line are the measured and computed values from Ref. 17, and the blue line corresponds to the CMDS results.

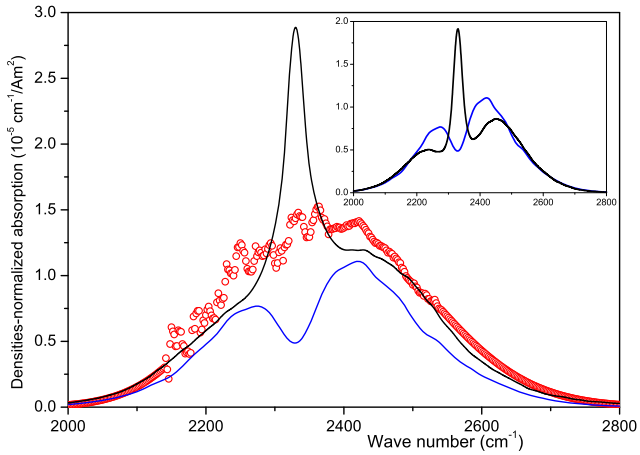

FIG. 4. Main panel: Comparison between the measured[17] (symbols) N_2–H_2O binary collision-induced absorption coefficient at 352 K and those computed using CMDS (black line) and the isotropic quantum model with the K_2 line shape (blue line). Inset: Computed CIA spectra obtained with the isotropic quantum model and K_2 line shape (blue line) and from CMDS neglecting the anisotropy of N_2–H_2O interactions (black line), both using on the same isotropic potential.

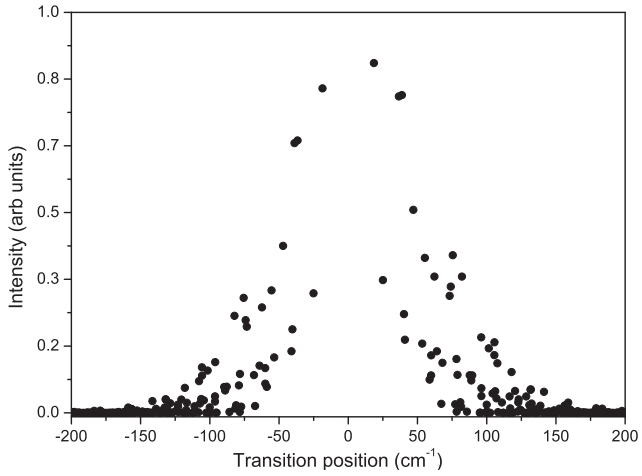

FIG. 5. Distribution of the intensities [i.e., $\rho_{J,Ka,Kc}(T)$ $\langle v=0,J,K_a',K_c'|\mu_{H_2O}|v=0,J,K_a,K_c\rangle^2$] of the $(v=0,J,K_a',K_c') \leftarrow (v=0,J,K_a,K_c)$ rotational Q transitions of H_2O obtained from the HITRAN2012 database.[44] See the end of the 2nd paragraph of Sec. III B for explanations on the transitions at negative frequencies.

obtained with the isotropic quantum model with the K_2 line shape (shown in the inset).

The fact that CMDSs lead to a N_2–H_2O CIA carrying a strong Q branch at its center (Figs. 3 and 4) is explained by the libration motion included in the classical rotation of H_2O. This motion leads, through the polarization of N_2, to an induced dipole that also librates. The Fourier transform of its ACF thus leads to a peak at frequency zero (that is then shifted to the frequency of the N_2 fundamental vibration; see Sec. III A 3) which is broadened due to the limited life time of the induced dipole. In the real (quantum) world, the situation is different and the Q transitions allowed by the H_2O static dipole are not centered at frequency zero. Indeed, Fig. 5 shows that the relevant transitions, extracted from the HITRAN2012 database,[44] are significantly shifted from $\sigma = 0$ cm^{-1}. The most intense ones peak below -20 cm^{-1} and above $+20$ cm^{-1} and one can thus expect that the N_2–H_2O CIA should not carry a peak at its center but, rather, a dip (as shown by the results of the isotropic quantum model with the K_2 line shape in Fig. 4).

In order to semi-empirically improve the CMDS predictions, the following procedure was applied: (i) A fit of the CMDS-calculated CIA in Fig. 3 was first made using three Lorentzians in order to represent the narrow central peak and the broader ones on its low and high frequency sides. Figure 6(a) shows that this leads to a quite satisfactory fit. (ii) In a second step, the Q branch was removed from the original CMDS spectrum by subtracting the corresponding Lorentzian, leading to the "Q-branch free" CIA shown by the blue line in Fig. 6(a) (the small peak in the central trough is due to a not fully perfect removal of the original Q branch). (iii) Finally, a more realistic contribution of the Q transitions of H_2O was calculated and added to the "Q-branch free" spectrum. It was obtained by simply summing of the transitions in Fig. 5, each having a Lorentzian shape. The half widths at half maximum used for this have been fixed to the value (23.3 cm^{-1}) obtained, in step (i), from the Lorentzian fit of the original Q branch. The overall area of the result was scaled to that (1.62×10^{-3} cm^{-2}/Am^2) retrieved from the same fit. The spectrum obtained from this exercise is compared with the measured one in Fig. 6(b). As can be seen, the agreement with the measurement is now quite good, although the predicted central trough between 2290 and 2370 cm^{-1} (which we believe is true) does not appear in the measurements. A possible explanation for this difference may be the perturbative absorption by the ν_3 band of traces of CO_2 present in the measured spectra[54] from which the N_2–H_2O CIA was retrieved.[17] Note that Fig. 6(b) presents not only a satisfactory prediction of the N_2–H_2O CIA spectrum but the very first one of the kind.

It is worth mentioning that the half-width obtained from the Lorentzian fit of the Q branch (23.3 cm^{-1}) is in very good agreement with that (24.5 cm^{-1}) of the K_2 line shape calculated for the relevant induced-dipole component (for which $\eta = 12.1$; see Table I). This agreement, together with the facts that K_2 line shape turns out to be close to Lorentzian and that the curves in the inset of Fig. 4 have practically the same

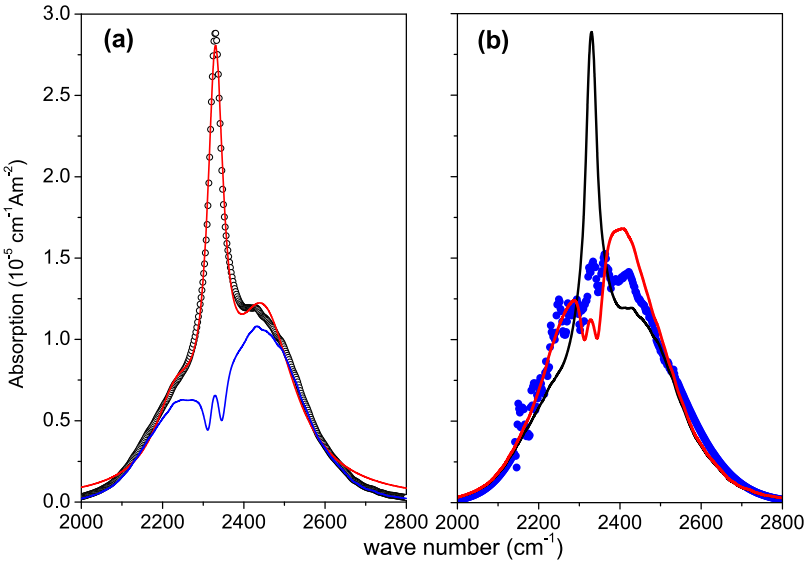

FIG. 6. N_2–H_2O binary collision-induced absorption coefficients at 352 K. (a) The circles represent the raw CMDS-calculated results and the red line their fit (see text) by three Lorentzians. The blue line is what is left from the former after subtraction of the fitted Lorentzian Q-branch. (b) The blue circles are the measured values[17] while the black and red lines denote the CMDS-computed CIA before and after the correction of the Q-branch (see text).

areas, further demonstrates the consistency of the CMDSs and quantum models when both use the isotropic approximation.

Finally, the fact that the peak and area of the N_2–H_2O CIA are much larger than those for pure N_2 can be explained by considering the dominant induction mechanisms, which are associated with the polarizability of N_2 in the fields of the H_2O dipole and N_2 quadrupole, respectively. For instance, the ratio of the amplitudes of the associated contribution to the absorption resulting from the isotropic part of N_2 polarizability scales as[35] $(\sqrt{2/3}R\,\langle v=0|\mu_{H_2O}\,|v=0\rangle/\langle v=0|\,\Theta_{N_2}|v=0\rangle)^2$, where R is the intermolecular distance. This leads, with $\langle v=0|\,\mu_{H_2O}\,|v=0\rangle = 0.73$ a.u. (see Sec. III A 2) and $\langle v=0|\,\Theta_{N_2}\,|v=0\rangle = -1.13$ a.u.,[35] to a ratio of $0.28R^2$ with R in atomic units. For a typical distance of 3.5 A, this leads to a factor of about 12. This enhancement in the N_2–H_2O pair is further increased by the anisotropy of the intermolecular potential, whose effect on the CIA is larger for this system that for pure N_2, as discussed above. Finally, the fact that the N_2 spectrum induced by collisions with H_2O is much broader than when collisions with N_2 are involved (see Fig. 3) simply comes from the much larger spectral spreading of the H_2O transitions (resulting from the larger rotational constant).

IV. CONSEQUENCES FOR TRANSMISSIONS IN THE EARTH'S ATMOSPHERE

A. Simulations and data used

In order to evaluate the influence of humidity on atmospheric absorption near 4 μm, we have simulated transmission spectra representative of those that can be recorded using ground-based solar occultation measurements. For this, vertical profiles of temperature, $T(z)$, and total pressure, $p_{Tot}(z)$, representative of a standard tropical atmosphere[55] were used [with temperatures of $T(0\,\text{km}) = 300$ K at ground level and of $T(17\,\text{km}) = 195$ K at the tropopause]. The CO_2 and N_2 volume mixing ratios were set constant and equal to 4×10^{-4} and 0.78, respectively, while standard vertical profiles[55] were used for all other species except water vapor. For H_2O, three profiles were constructed, with no water vapor above the tropopause and values in the troposphere corresponding to constant percentages of humidity of 0%, 20%, and 100%. In other words, the H_2O mole fraction at altitude z < 17 km is given by $x_{H_2O}(z) = A\times p_{Sat}\,[T(z)]\,/p_{Tot}(z)$ with A = 0, 0.2, or 1.0, where $p_{Sat}(T)$ is the saturation pressure at temperature T. In the 100% humidity case, the H_2O fraction at ground level is 3.5% and the total precipitable water inside a vertical column is 6.7 g/cm^2 (i.e., 67 mm).

The atmospheric absorbance integrated (by steps of 1 km) over a vertical column was computed in the 2000-2800 cm^{-1} spectral region by taking the contributions of CO_2, N_2, H_2O, N_2O, CH_4, and CO into account. The needed line positions and integrated intensities were all taken from the HITRAN2012 database.[44] Voigt line shapes were retained with a cutoff 3 cm^{-1} away from line-centers, except for CO_2 transitions for which the corrective χ factors of Refs. 56 and 18 were applied for CO_2-(dry air) and CO_2–H_2O collisions, respectively. For all species, dry air line-broadening coefficient from HITRAN2102 was used, except for CO_2 for which the broadening by H_2O was taken into account using the data of Ref. 57. The continuum absorption of water vapor was disregarded. This was done for simplicity, but also because its contribution between 2200 and 2800 cm^{-1} is relatively small[10,54] and still uncertain (see Secs. 3.5.4 and 4.3 of Ref. 58). For the N_2 CIA in dry air, a refined version of the software+data package of Ref. 59, now extending up to 2830 cm^{-1} and down to 1930 cm^{-1}, was created by using the data of Ref. 47. For the N_2–H_2O CIA, a simple temperature-dependent model was constructed, between 1930 and 2830 cm^{-1}, from CMDS-calculated values at 250, 300, and 350 K. The raw CMDSs were used and the semi-empirical correction discussed at the end of Sec. III C was not applied. As seen from Fig. 3, this gives a good enough (for the present study) representation of this CIA, except in the central region of the band. Fortunately, this is of no consequences for the present simulations since the atmospheric transmission is negligible in this region (see below) thanks to the very strong absorption by CO_2. More refined data for the N_2–H_2O CIA will be constructed and used in a future study for comparisons between calculated and measured atmospheric spectra.

B. Results and discussion

The computed atmospheric high-resolution absorbances (integrated over a vertical column) of CO_2 and N_2 around 4.3 μm are plotted in Fig. 7 for the fully dry and fully humid cases. As can be seen, humidity does have a significant influence, as could be expected from the results of Secs. II and III. In order to be more specific, let us denote by $A^D(\sigma)$ and $A^H(\sigma)$ the dry and humid atmospheric absorbances in Fig. 7, with which the difference between the associated transmissions for an airmass of M is $\exp\left[-A^D(\sigma)M\right] - \exp\left[-A^H(\sigma)M\right]$. This difference would be detectable in measurements provided that it is greater than a few 10^{-2}. This requires to simultaneously have $\left[A^H(\sigma) - A^D(\sigma)\right]M$ greater than a few 10^{-2} and $\exp\left[-A^D(\sigma)M\right]$ not too small. It can easily be concluded from Fig. 7 that, for airmasses between 1 and 10, there are several

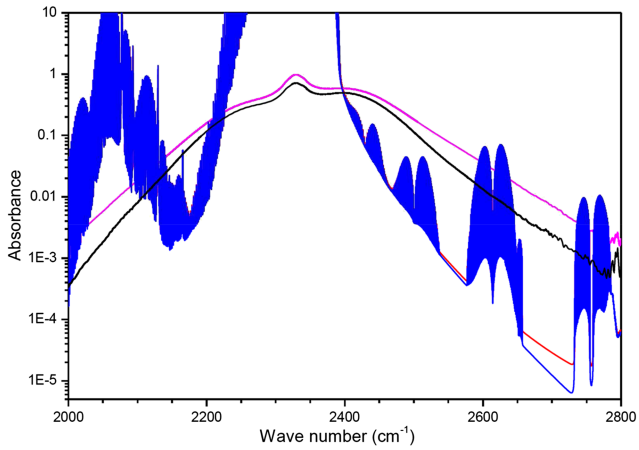

FIG. 7. Computed CO_2 and N_2 absorbances, integrated over a vertical atmospheric column. The black and magenta lines are for N_2 in atmospheres with 0% and 100% humidity (see Sec. IV A), respectively, while the corresponding results for CO_2 are the blue and red lines.

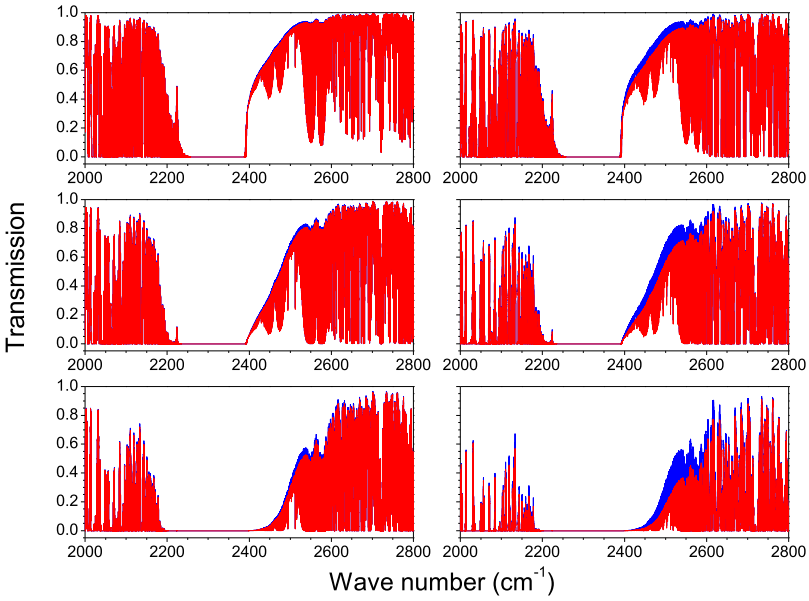

FIG. 8. Simulated transmission spectra of atmospheres with 20% (left) and 100% (right) humidity for airmasses of 1, 3, and 9 (from top down). The red and blue curves have been obtained with and without taking into account the influence of humidity on the CO_2 line wings and the N_2 CIA, respectively.

regions where the effects of humidity on atmospheric transmissions could be observable, as is confirmed later. Note that this statement applies to the N_2 contribution and not to that of the CO_2 band wings where the effects are too small and completely masked by the N_2 absorption.

The differences in Fig. 7 between the absorbances for the dry and humid atmospheres in the N_2 CIA and the wing of the CO_2 ν_3 band can be quantitatively explained as follows. In these regions, the absorbance at wave number σ for species X is given by

$$A_X(\sigma) = \int_0^\infty dz \{n_X(z) n_{air}(z) C_{X\text{ - air}}[\sigma, T(z)] + n_X(z) n_{H_2O}(z) C_{X\text{ - }H_2O}[\sigma, T(z)]\}, \quad (3)$$

where $T(z)$ and $n_Y(z)$ denote the temperature and the density of species Y (=N_2, CO_2, air, or H_2O) at altitude z, respectively, while $C_{X\text{-}Y}(\sigma,T)$ is the normalized (i.e., divided by the product of the densities of X and Y) binary absorption coefficient due to species X colliding with Y (e.g., Figs. 1 and 3). If one assumes, for simplicity, that the latter is independent on temperature (quite reasonable), the relative difference between the humid and dry atmospheres absorbances for species X is

$$\frac{A_X^H(\sigma) - A_X^D(\sigma)}{A_X^D(\sigma)} = \frac{C_{X\text{ - }H_2O}(\sigma)}{C_{X\text{ - air}}(\sigma)} \frac{\int_0^\infty n_X(z) n_{H_2O}(z) dz}{\int_0^\infty n_X(z) n_{air}(z) dz}. \quad (4)$$

For the tropical atmosphere described in Sec. IV A, the (last) ratio of integrated densities products in Eq. (4) is equal to 0.016 in the 100% humidity case. It is then quite easy to see that the effects of humidity shown in Fig. 7 are consistent with the difference between the pure N_2 and N_2–H_2O CIAs in Fig. 3 and the fact that the H_2O-broadened far wing of the CO_2 ν_3 band is much larger[17] than that for CO_2 in dry air. For a factor of ten between $C_{X\text{ - }H_2O}(\sigma, T)$ and $C_{X\text{ - air}}(\sigma, T)$, for instance, the relative error on the absorbance induced by neglecting the effect of humidity is 16%.

Figure 8 displays synthetic atmospheric transmissions spectra for various values of the airmass (i.e., of the solar zenith angle in ground-based solar-occultation measurements) and humidity. It enables us to compare results obtained with and without the inclusion of the influence of water vapor on the spectra of CO_2 and N_2. As can be seen, this influence is often obvious and likely detectable in adapted measurements, although there are parts of the spectrum where it is masked by the absorption by other gases. It is the case on the low and high frequency sides of the displayed window where the absorption is dominated by lines of H_2O, while N_2O is responsible for the P and R branches around 2469 and 2560 cm^{-1}. Finally, analysis shows that, as predicted from Fig. 7, the influence of H_2O on the wings of the CO_2 bands is too small or masked to be detectable and that the differences between the transmissions in Fig. 8 are due to the N_2 CIA only. Checking these prediction using real atmospheric spectra will be our next step on this research topic.

V. CONCLUSION AND DIRECTIONS FOR FUTURE STUDIES

The results presented in this paper show that classical molecular dynamics simulations can be reliably used for predictions of the effects of collisions with water vapor on the absorption in both the wings of the CO_2 ν_3 band and the fundamental collision-induced band of N_2 (provided that, for N_2, the simple to implement correction described at the end of Sec. III C is made). This opens the route for the creation of relevant and reliable data at temperatures of the Earth's atmosphere for which laboratory measurements are very difficult, if not impossible, to carry. This is of practical interest since simulations show that neglecting the effect of humidity in computations of atmospheric absorption by N_2 around 4 μm leads to a significant overestimation of the transmission. A study, in which predictions and the available measurements will be used to construct the best possible model, will be the subject of a future work, together with its subsequent test by comparisons between measured and calculated spectra of the Earth's atmosphere. Note that while we have shown that data on the absorption continua of CO_2–H_2O mixtures are not needed for the Earth's atmosphere (at least near 4 μm),

they are of crucial importance for planetology research. It is the case for studies of the current or past climates of several planets with atmospheres containing significant amounts of both CO_2 and H_2O (e.g., Refs. 61–63 and those therein), for which including both the effects of collisions with H_2O on CO_2 absorption and of collisions with CO_2 on H_2O spectra[60] is required.

[1] I. E. Gordon, L. S. Rothman, C. Hill, R. V. Kochanov, Y. Tan, P. F. Bernath, M. Birk, V. Boudon, A. Campargue, K. V. Chance, B. J. Drouin, J.-M. Flaud, R. R. Gamache, J. T. Hodges, D. Jacquemart, V. I. Perevalov, A. Perrin, K. P. Shine, M. A. H. Smith, J. Tennyson, G. C. Toon, H. Tran, V. G. Tyuterev, A. Barbe, A. G. Császár, V. M. Devi, T. Furtenbacher, J. J. Harrison, J.-M. Hartmann, A. Jolly, T. J. Johnson, T. Karman, I. Kleiner, A. A. Kyuberis, J. Loos, O. M. Lyulin, S. T. Massie, S. N. Mikhailenko, N. Moazzen-Ahmadi, H. S. P. Müller, O. V. Naumenko, A. V. Nikitin, O. L. Polyansky, M. Rey, M. Rotger, S. W. Sharpe, K. Sung, E. Starikova, S. A. Tashkun, J. Vander Auwera, G. Wagner, J. Wilzewski, P. Wcisło, S. Yu, and E. J. Zak, J. Quant. Spectrosc. Radiat. Transfer **203**, 3 (2017).

[2] N. Jacquinet-Husson, R. Armante, N. A. Scott, A. Chédin, L. Crépeau, C. Boutammine, A. Bouhdaoui, C. Crevoisier, V. Capelle, C. Boonne, N. Poulet-Crovisier, A. Barbe, D. Chris Benner, V. Boudon, L. R. Brown, J. Buldyreva, A. Campargue, L. H. Coudert, V. M. Devi, M. J. Down, B. J. Drouin, A. Fayt, C. Fittschen, J. M. Flaud, R. R. Gamache, J. J. Harrison, C. Hill, Hodnebrog, S. M. Hu, D. Jacquemart, A. Jolly, E. Jiménez, N. N. Lavrentieva, A. W. Liu, L. Lodi, O. M. Lyulin, S. T. Massie, S. Mikhailenko, H. S. P. Müller, O. V. Naumenko, A. Nikitin, C. J. Nielsen, J. Orphal, V. I. Perevalov, A. Perrin, E. Polovtseva, A. Predoi-Cross, M. Rotger, A. A. Ruth, S. S. Yu, K. Sung, S. A. Tashkun, J. Tennyson, V. G. Tyuterev, J. Vander Auwera, B. A. Voronin, and A. Makie, J. Mol. Spectrosc. **327**, 31 (2016).

[3] T. Delahaye, X. Landsheere, E. Pangui, F. Huet, J.-M. Hartmann, and H. Tran, J. Mol. Spectrosc. **326**, 17 (2016).

[4] T. Delahaye, X. Landsheere, E. Pangui, F. Huet, J.-M. Hartmann, and H. Tran, J. Quant. Spectrosc. Radiat. Transfer **173**, 40 (2016).

[5] T. Delahaye, X. Landsheere, E. Pangui, F. Huet, J.-M. Hartmann, and H. Tran, J. Quant. Spectrosc. Radiat. Transfer **184**, 316 (2016).

[6] J. S. Wilzewski, I. E. Gordon, R. V. Kochanov, C. Hill, and L. S. Rothman, J. Quant. Spectrosc. Radiat. Transfer **168**, 193 (2016).

[7] OCO-2 (Orbiting Carbon Observatory-2), https://directory.eoportal.org/web/eoportal/satellite-missions/o/oco-2, and references therein.

[8] MERLIN (MEthane Remote Sensing LIdar Mission) Minisatellite, https://directory.eoportal.org/web/eoportal/satellite-missions/m/merlin and references therein.

[9] MicroCarb (Carbon Dioxide Monitoring Mission), https://directory.eoportal.org/web/eoportal/satellite-missions/m/microcarb and references therein.

[10] E. J. Mlawer, V. H. Payne, J. Moncet, J. S. Delamere, M. J. Alvarado, and D. C. Tobin, Philos. Trans. R. Soc., A **370**, 2520 (2012).

[11] P.-Y. Foucher, A. Chédin, G. Dufour, V. Capelle, C. D. Boone, and P. F. Bernath, Atmos. Chem. Phys. **9**, 2873 (2009).

[12] P.-Y. Foucher, A. Chédin, R. Armante, C. D. Boone, C. Crevoisier, and P. F. Bernath, Atmos. Chem. Phys. **11**, 2455 (2011).

[13] C. E. Sioris, C. D. Boone, R. Nassar, K. J. Sutton, I. E. Gordon, K. A. Walker, and P. F. Bernath, Atmos. Meas. Tech. **7**, 2243 (2014).

[14] O. Absil, J. Milli, D. Mawet, A. M. Lagrange, J. Girard, G. Chauvin, A. Boccaletti, C. Delacroix, and J. Surdej, Astron. Astrophys. **559**, L12 (2013).

[15] V. A. Krasnopolsky, D. A. Belyaev, I. E. Gordon, G. Li, and L. S. Rothman, Icarus **224**, 57 (2013).

[16] R. E. Johnson, T. S. Stallard, H. Melin, J. D. Nichols, and S. W. H. Cowley, J. Geophys. Res.: Space Phys. **122**, 7599, https://doi.org/10.1002/2017ja024176 (2017).

[17] Y. I. Baranov, I. A. Buryak, S. E. Lokshtanov, V. A. Lukyanchenko, and A. A. Vigasin, Philos. Trans. R. Soc., A **370**, 2691 (2012).

[18] H. Tran, M. Turbet, P. Chelin, and X. Landsheere, "Measurements and modelling of absorption by $CO_2 + H_2O$ mixture in the far line wings of the ν_3 CO_2 band," Icarus (in press).

[19] Y. I. Baranov, J. Quant. Spectrosc. Radiat. Transfer **175**, 100 (2016).

[20] N. H. Ngo, H. Tran, and R. R. Gamache, J. Chem. Phys. **136**, 154310 (2012).

[21] N. H. Ngo, H. Tran, R. R. Gamache, D. Bermejo, and J.-L. Domenech, J. Chem. Phys. **137**, 064302 (2012).

[22] J.-M. Hartmann and C. Boulet, J. Chem. Phys. **134**, 184312 (2011).

[23] J.-M. Hartmann, H. Tran, N. H. Ngo, X. Landsheere, P. Chelin, X. Lu, A. W. Liu, S. M. Hu, L. Gianfrani, G. Casa, A. Castrillo, M. Lepère, Q. Delière, M. Dhyne, and L. Fissiaux, Phys. Rev. A **87**, 013403 (2013).

[24] E. M. Mas, R. Bukowski, K. Szalewicz, G. C. Groenenboom, P. E. S. Wormer, and A. van der Avoird, J. Chem. Phys. **113**, 6687 (2000).

[25] C. S. Murthy, S. E. O'Shea, and L. R. McDonald, Mol. Phys. **50**, 531 (1983).

[26] L. J. Karssemeijer, G. A. de Wijs, and H. M. Cuppen, Phys. Chem. Chem. Phys. **16**, 15630 (2014).

[27] J.-M. Hartmann, C. Boulet, and D. Jacquemart, J. Chem. Phys. **134**, 094316 (2011).

[28] C. Leforestier, R. H. Tipping, and Q. Ma, J. Chem. Phys. **132**, 164302 (2010).

[29] D. Spelsberg and W. Meyer, J. Chem. Phys. **101**, 1282 (1994).

[30] G. Maroulis, Chem. Phys. Lett. **289**, 403 (1998).

[31] A. Hu, D. M. York, and T. K. Woo, J. Mol. Struct. **591**, 255 (2002).

[32] V. M. Devi, B. Fridovich, G. D. Jones, and D. G. S. Snyder, J. Mol. Spectrosc. **105**, 61 (1984).

[33] C. Cousin, R. Le Doucen, J.-P. Houdeau, C. Boulet, and A. Henry, Appl. Opt. **25**, 2434 (1986).

[34] A. Haskopoulos and G. Maroulis, Chem. Phys. Lett. **417**, 235 (2006).

[35] L. Frommhold, *Collision Induced Absorption in Gases*, Cambridge Monographs on Atomic, Molecular, and Chemical Physics (Cambridge University Press, Cambridge, 2006), pp. 191–193.

[36] J.-M. Hartmann, C. Boulet, H. Tran, and M. T. Nguyen, J. Chem. Phys. **133**, 144313 (2010).

[37] H. Tran, C. Boulet, S. Stefani, M. Snels, and G. Piccioni, J. Quant. Spectrosc. Radiat. Transfer **112**, 925 (2011).

[38] J.-M. Hartmann, C. Boulet, and G. C. Toon, J. Geophys. Res.: Atmos. **122**, 2419, https://doi.org/10.1002/2016jd025677 (2017).

[39] J. D. Poll and J. L. Hunt, Can. J. Phys. **54**, 461 (1976).

[40] A. Brown, R. H. Tipping, and M. Maté, J. Mol. Spectrosc. **204**, 153 (2000).

[41] A. Brown and R. H. Tipping, J. Mol. Spectrosc. **205**, 319 (2001).

[42] A. Brown, and R. H. Tipping, in *Weakly Interacting Molecular Pairs: Unconventional Absorbers of Radiation in the Atmosphere*, NATO Science Series (Series IV: Earth and Environmental Sciences), edited by C. Camy-Peyret and A. A. Vigasin (Springer, Dordrecht, 2003), Vol. 27.

[43] J. Boissoles, R. H. Tipping, and C. Boulet, J. Quant. Spectrosc. Radiat. Transfer **51**, 615 (1994).

[44] L. S. Rothman, I. E. Gordon, Y. Babikov, A. Barbe, D. Chris Benner, P. F. Bernath, M. Birk, L. Bizzocchi, V. Boudon, L. R. Brown, A. Campargue, K. Chance, E. A. Cohen, L. H. Coudert, V. M. Devi, B. J. Drouin, A. Fayt, J. M. Flaud, R. R. Gamache, J. J. Harrison, J. M. Hartmann, C. Hill, J. T. Hodges, D. Jacquemart, A. Jolly, J. Lamouroux, R. J. Le Roy, G. Li, D. A. Long, O. M. Lyulin, C. J. Mackie, S. T. Massie, S. Mikhailenko, H. S. P. Müller, O. V. Naumenko, A. V. Nikitin, J. Orphal, V. Perevalov, A. Perrin, E. R. Polovtseva, C. Richard, M. A. H. Smith, E. Starikova, K. Sung, S. Tashkun, J. Tennyson, G. C. Toon, V. G. Tyuterev, and G. Wagner, J. Quant. Spectrosc. Radiat. Transfer **130**, 4 (2013).

[45] G. Birnbaum and E. R. Cohen, Can. J. Phys. **54**, 593 (1976).

[46] J. L. Hunt and J. D. Poll, Can. J. Phys. **56**, 950 (1978).

[47] Y. I. Baranov, W. J. Lafferty, and G. T. Fraser, J. Mol. Spectrosc. **233**, 160 (2005).

[48] C. Richard, I. E. Gordon, L. S. Rothman, M. Abel, L. Frommhold, M. Gustafsson, J.-M. Hartmann, C. Hermans, W. J. Lafferty, G. S. Orton, K. M. Smith, and H. Tran, J. Quant. Spectrosc. Radiat. Transfer **113**, 1276 (2012).

[49] G. Moreau, J. Boissoles, R. Le Doucen, C. Boulet, R. H. Tipping, and Q. Ma, J. Quant. Spectrosc. Radiat. Transfer **69**, 245 (2001).

[50] A. Borysow and M. Moraldi, Phys. Rev. Lett. **68**, 3686 (1992).

[51] B. Bussery-Honvault and J.-M. Hartmann, J. Chem. Phys. **140**, 054309 (2014).

[52] T. Karman, E. Miliordos, K. L. C. Hunt, G. C. Groenenboom, and A. van der Avoird, J. Chem. Phys. **142**, 084306 (2015).

[53] M. Gruszka and A. Borysow, Mol. Phys. **93**, 1007 (1998).

[54] Y. I. Baranov, J. Quant. Spectrosc. Radiat. Transfer **112**, 2281 (2011).

[55] U.S. Government Printing Office, *U.S. Standard Atmosphere* (U.S. Government Printing Office, Washington, DC, 1976).

[56] M.-Y. Perrin and J.-M. Hartmann, J. Quant. Spectrosc. Radiat. Transfer **42**, 311 (1989).

[57] K. Sung, L. R. Brown, R. A. Toth, and T. Crawford, Can. J. Phys. **87**, 469 (2009).

[58]J.-M. Hartmann, H. Tran, R. Armante, C. Boulet, A. Campargue, F. Forget, L. Gianfrani, I. Gordon, S. Guerlet, M. Gustafsson, J. Hodges, S. Kassi, D. Lisak, F. Thibault, and G. C. Toon, "Recent advances in collisional effects on spectra of molecular gases and their practical consequences," J. Quant. Spectrosc. Radiat. Transfer (submitted).
[59]W. J. Lafferty, A. M. Solodov, A. Weber, W. B. Olson, and J.-M. Hartmann, Appl. Opt. **35**, 5911 (1996).
[60]J. B. Pollack, J. B. Dalton, D. Grinspoon, R. B. Wattson, R. Freedman, D. Crisp, D. A. Allen, B. Bézard, C. DeBergh, L. P. Giver, Q. Ma, and R. H. Tipping, Icarus **103**, 1 (1993).
[61]L. T. Elkins-Tanton, Earth Planet. Sci. Lett. **271**, 181 (2008).
[62]T. L. Segura, O. B. Toon, A. Colaprete, and K. Zahnle, Science **298**, 1977 (2002).
[63]R. M. Ramirez, R. K. Kopparapu, V. Lindner, and J. F. Kasting, Astrobiology **14**, 714 (2014).